

Transmission in graphene through a double laser barrier

Rachid El Aitouni,¹ Miloud Mekkaoui,¹ and Ahmed Jellal^{1,2,*}

¹Laboratory of Theoretical Physics, Faculty of Sciences,
Chouaib Doukkali University, PO Box 20, 24000 El Jadida, Morocco

²Canadian Quantum Research Center, 204-3002 32 Ave Vernon, BC V1T 2L7, Canada

We study the tunneling behavior of Dirac fermions in graphene subjected to a double barrier potential profile created by spatially overlapping laser fields. By modulating the graphene sheet with an oscillating structure formed from two laser barriers, we aim to understand how the transmission of Dirac fermions is influenced by such a light-induced electric potential landscape. Using the Floquet method, we determine the eigenspinors of the five regions defined by the barriers applied to the graphene sheet. Applying the continuity of the eigenspinors at barrier edges and using the transfer matrix method, we establish the transmission coefficients. These allow us to show that oscillating laser fields generate multiple transmission modes, including zero-photon transmission aligned with the central band ε and photon-assisted transmission at sidebands $\varepsilon + l\varpi$, with $l = 0, \pm 1, \dots$ and frequency ϖ . For numerical purposes, our attention is specifically directed towards transmissions related to zero-photon processes ($l = 0$), along with processes involving photon emission ($l = 1$) and absorption ($l = -1$). We find that transmission occurs only when the incident energy is above the threshold energy $\varepsilon > k_y + 2\varpi$, with transverse wave vector k_y . We find that the variation in distance d_1 separating two barriers of widths $d_2 - d_1$ suppresses one transmission mode. Additionally, we show that an increase in laser intensity modifies transmission sharpness and amplitude.

PACS numbers: 78.67.Wj, 05.40.-a, 05.60.-k, 72.80.Vp

KEYWORDS: Graphene, two laser barriers, Dirac equation, transmission mode, Klein tunneling.

I. INTRODUCTION

Graphene is a one-atom thick, two-dimensional carbon material in which carbon atoms are arranged in a hexagonal honeycomb lattice [1, 2]. It was first isolated in 2004 [3] and has since demonstrated remarkable electronic and optical properties [4]. Graphene exhibits massless Dirac fermion behavior near the Fermi level [5] and the quantum Hall effect [6, 7], with charge carriers achieving high mobilities [8, 9] approaching 1/300 the speed of light. In addition, graphene possesses attractive photonic attributes such as broadband absorption of approximately 2.3% of incident ultraviolet and infrared radiation [10]. Its properties are described by tight-binding model [11], with the dispersion relation exhibiting linear bands near the Dirac points [12]. This implies nearly frictionless transport, as fermions readily traverse the conduction and valence bands. However, robust tunneling even at sub-barrier energies, known as the Klein tunneling effect, hindered graphene's integration into devices [13, 14]. Experiments later verified Klein tunneling, where normally incident fermions transmit through barriers regardless of width or potential [15].

Strategies to modulate Dirac fermion flow, such as mitigating Klein tunneling through barrier designs, could facilitate graphene's incorporation into electronics. Several methods have been developed, among them we cite depositing the graphene sheet onto a substrate [16], doping it with another type of atom [17], deforming the sheet [18, 19], and applying an external electric, magnetic, or laser field. Klein tunneling is consistently observed in simple barrier. However, by adding a second barrier, the number of transmission oscillations increases due to the additional resonance caused by the quasi-confined states between the two barriers [20–22]. Confining fermions with a magnetic barrier results in the quantization of the energy spectrum [23]. Despite this confinement, these fermions still exhibit Klein tunneling, highlighting a persistent and notable phenomenon. Remarkably, for a sequence of N magnetic barriers, the transparency of transmission increases progressively with the growing value of N [24, 25]. The quantification of the energy spectrum can also occur when dealing with a time-oscillating barrier [26–30], giving rise to the emergence of multiple transmission modes [31, 32]. The process of laser irradiation on graphene induces photon exchange between the graphene fermions and the barrier (laser field). Notably, increasing the intensity of the laser field has been demonstrated to effectively diminish overall transmission [31, 32]. In a related context, it has been observed that irradiating graphene subjected to an inclined potential barrier results in null transmission [33], leading to the complete confinement of fermions. This phenomenon is identified as anti-Klein tunneling. Furthermore, the introduction of a magnetic field, along with a laser field, allows for the suppression of processes with zero photon exchange and the activation of processes involving photon exchange [34].

* ahmed.jellal@gmail.com

We investigate the transmission of Dirac fermions through double laser barrier structures incorporated into a graphene sheet. The modulation of graphene with nanoscale laser potentials serves as a focal point for understanding how Dirac fermion transport is influenced by the induced photon-assisted tunneling dynamics within the barrier configuration. This exploration of light-matter interactions at the nano-scale interface between photonics and electronics has the potential to facilitate future control of emergent phenomena in graphene and other van der Waals materials. To achieve our research objectives, we initiate the analysis by determining the eigenspinors within each region. This is accomplished by solving the eigenvalue equation using the Floquet method [35]. Subsequently, we apply boundary conditions at the interfaces of the double barriers and use the transfer matrix approach to derive all transmission modes. In our numerical simulations, we specifically focus on transmissions involving zero photon exchange ($l = 0$), as well as photon-assisted processes encompassing emission ($l = 1$) or absorption ($l = -1$) of photons. This selective focus on first-order sideband transition modes streamlines the computational treatment while still providing valuable insights into the intricate interplay between photon-assisted tunneling and Dirac fermion transport, modulated by the laser barrier structure. We demonstrate that successful transmission occurs when the energy satisfies the condition $\varepsilon > k_y + 2\varpi$. This implies that fermions need to surpass a certain energy threshold to traverse the barrier. The manipulation of the distance between the two barriers and the adjustment of the barrier width allow for the modification of the amplitudes of two transmission modes or the suppression of one. Moreover, the number of transmission oscillations increases across all regions, attributed to additional resonances arising from quasi-confined states between the two barriers. We illustrate that the intensity of the laser field directly influences both the amplitude of transmission and the overall transmission process. Importantly, our findings reveal that, irrespective of amplitude, the transmission modes exhibit sinusoidal variations.

The paper is organized as follows: In Sec. II, we establish a theoretical model describing the system, which consists of five regions. We solve the eigenvalue equation to determine the eigenspinors associated with each region. In Appendix A, we apply the boundary conditions and utilize the current density to derive all transmission modes using the transfer matrix approach. By focusing on the first three modes, we present our numerical results and discuss the fundamental features of the system in Sec. III. We then conclude our findings in Sec. IV.

II. THEORETICAL MODEL

We consider a graphene sheet partitioned into five regions, denoted by $j = 1, 2, \dots, 5$. In regions 1, 3, and 5, pristine graphene is maintained. However, in regions 2 and 4, we introduce two distinct laser fields characterized by amplitudes A_2 and A_4 , respectively, and phase-shifted by an angle β , as depicted in Fig. 1. We want to highlight that our portrayal of the laser field as a step-like potential with nanometer resolution is a deliberately simplified modeling approach chosen for analytical tractability. This intentional simplification aims to capture essential aspects of the interaction while recognizing its inherently idealized nature. Our objective is not to precisely replicate real-world laser fields at the atomic scale but rather to establish a theoretical framework for examining the impact of double laser barriers on transmission in graphene. While our model provides valuable conceptual insights, we acknowledge the necessity for a more careful consideration of practical limitations. It is important to recognize that the idealization of perfectly rectangular laser barriers with nanometer resolution surpasses current experimental capabilities. Nevertheless, the scientific community is experiencing the development of innovative nanophotonics techniques that have the potential to shape optical fields at relevant length scales. In particular, progress in plasmonic nanostructures and metasurfaces presents promising avenues for localizing light in subwavelength regions through surface plasmons. Describing a laser field applied to graphene in the context of a step-like potential with nanometer resolution and modulating it at the same scale requires a multifaceted approach. Theoretical exploration entails utilizing quantum mechanical models, such as tight-binding or density functional theory, to gain a comprehensive understanding of the electronic behavior of graphene under the influence of a laser field [1]. The notion of a step-like potential in laser-graphene interactions is based on the potential landscape experienced by electrons in the graphene lattice during laser irradiation, driven by the transfer of energy from the laser field [36]. To achieve nanometer resolution in describing a laser field on graphene, sophisticated experimental techniques become paramount. Instruments such as scanning tunneling microscopy (STM) and atomic force microscopy (AFM) enable researchers to investigate electronic and structural changes at the nanoscale with unprecedented precision [37]. Furthermore, modulating a laser field at the nanoscale on graphene entails external control mechanisms and dynamic tuning. Techniques like plasmonic modulation and the application of tailored external fields offer effective means to influence the laser-graphene interaction at the nanometer scale [38]. In summary, the comprehensive description of a laser field applied to graphene, considering both step-like potential changes and nanometer-scale modulation, requires an integrated approach that combines theoretical insights, advanced experimental techniques, and external control mechanisms. This holistic strategy is essential for advancing our understanding of laser-graphene interactions and their potential applications.

We emphasize that graphene is a highly relevant material due to its exceptional electronic, mechanical, and thermal

properties [1]. However, it is not the only relevant system in the field of materials science and condensed matter physics. Researchers have explored a wide range of two-dimensional materials and nanostructures, each possessing unique properties and potential applications. Other relevant systems include transition metal dichalcogenides (TMDs) like molybdenum disulfide (MoS₂) and tungsten diselenide (WSe₂) [39, 40], as well as other carbon allotropes like carbon nanotubes and fullerenes [41]. These materials exhibit distinct characteristics that make them suitable for various technological advancements.

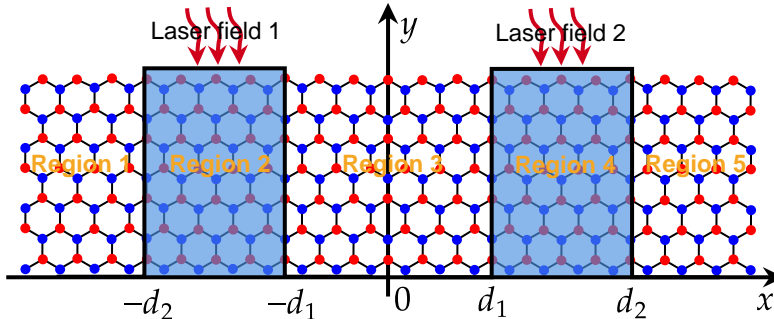


FIG. 1. (Color online) A diagram illustrates a graphene sheet with two laser barriers, each of width $d_2 - d_1$, creating a system divided into five distinct regions.

To conduct a theoretical analysis of the present system, we construct a Hamiltonian that incorporates all the mentioned constraints. It can be expressed as follows:

$$H_j = v_F \vec{\sigma} \cdot \left(\vec{p} + \frac{e}{c} \vec{A}_j(t) \right), \quad j = 1, 2, \dots, 5 \quad (1)$$

where v_F is the Fermi velocity, $\vec{\sigma}$ are the Pauli matrices (σ_x, σ_y), and $\vec{p} = (p_x, p_y)$ is the momentum. In the electric dipole approximation [42], $\vec{A}_j(t)$ represents the vector potential corresponding to the laser field

$$\vec{A}_j(t) = (0, A_j \cos \Phi_j, 0) \quad (2)$$

with Φ_j and A_j being the phase and amplitude of the laser field in each region

$$\Phi_j = \begin{cases} \Phi_1 = 0 \\ \Phi_2 = \omega t \\ \Phi_3 = 0 \\ \Phi_4 = \omega t + \beta \\ \Phi_5 = 0 \end{cases}, \quad A_j = \begin{cases} A_1 = 0, & x < -d_2 \\ A_2, & -d_2 < x < -d_1 \\ A_3 = 0, & -d_1 < x < d_1 \\ A_4, & d_1 < x < d_2 \\ A_5 = 0, & x > d_2 \end{cases} \quad (3)$$

while the parameter β denotes a phase shift. This potential generates the oscillating electric field $\vec{F}_j(t) = F_j \sin \Phi_j \vec{u}$ of amplitude $F_j = \omega A_j$ and \vec{u} is the unit vector along the polarization direction of the field (the y -axis).

To determine the wave function corresponding to each region, we solve the wave equation by spitting the Hamiltonian (1) into spatial H_0 and temporal \tilde{H}_j parts, i.e., $H_j = H_0 + \tilde{H}_j$, with

$$H_0 = v_F (\sigma_x p_x + \sigma_y p_y), \quad \tilde{H}_j = v_F \sigma_y A_j(t). \quad (4)$$

Given that H_0 is time-independent and \tilde{H}_j is coordinate-independent, the total eigenspinors $\Psi_j(x, y, t) = \psi_j(x, y) \phi_j(t)$ can be represented as a tensor product of the two eigenvectors $\psi_j(x, y) = \begin{pmatrix} \varphi_j^+(x, y) \\ \varphi_j^-(x, y) \end{pmatrix}$ and $\phi_j(t)$ associated with H_0 and \tilde{H}_j , respectively. In the framework of the Floquet approximation [43, 44], the temporal part is expressed as $\phi_j(t) = \chi_j(t) e^{-i\varepsilon t}$ (in system unit $\hbar = e = c = 1$) associated with the Floquet energy $\varepsilon = \frac{E}{v_F}$, with $\chi_j(t)$ being a periodic function over time. The eigenvalue equation $H_j \Psi_j(x, y, t) = E \Psi_j(x, y, t)$ yields

$$[\partial_x + k_y - A_j \cos \Phi_j] \varphi_j^-(x, y) \chi_j(t) = \varphi_j^+(x, y) \frac{\partial}{\partial t} \chi_j(t) \quad (5)$$

$$[\partial_x - k_y + A_j \cos \Phi_j] \varphi_j^+(x, y) \chi_j(t) = \varphi_j^-(x, y) \frac{\partial}{\partial t} \chi_j(t). \quad (6)$$

Unfortunately, It is not possible to determine the three unknown functions, $(\varphi_j^+, \varphi_j^-, \chi_j)$, from these two equations. Thus, it is necessary to resort to some approximation. In this context, we use an iterative method to solve for the three variables [32]. As a first approximation, we assume that $u_A(x)$ and $u_B(x)$ satisfy the coupled differential equations inside the barrier region without laser influence. Under this assumption, (5) and (6) to the following

$$-A_j \cos \Phi_j \varphi_j^-(x, y) \chi_j(t) = \varphi_j^+(x, y) \frac{\partial}{\partial t} \chi_j(t) \quad (7)$$

$$A_j \cos \Phi_j \varphi_j^+(x, y) \chi_j(t) = \varphi_j^-(x, y) \frac{\partial}{\partial t} \chi_j(t) \quad (8)$$

which gives rise to the following second order differential equation

$$(\partial_t^2 + \omega \tan \Phi_j \partial_t + A_j^2 \cos^2 \Phi_j) \chi_j(t) = 0 \quad (9)$$

having the solution

$$\chi_j(t) = e^{-i\alpha \sin \Phi_j} = \sum_{m=-\infty}^{+\infty} J_m(\alpha_j) e^{-m\Phi_j} \quad (10)$$

where J_m is the Bessel functions, and $\alpha_j = \frac{F_j}{\omega^2}$. Combing all to write the eigenspinors of H_j as

$$\Psi_j(x, y, t) = \psi_j(x, y) \sum_{m=-\infty}^{+\infty} J_m(\alpha_j) e^{-i(\varepsilon t + m\Phi_j)}. \quad (11)$$

To obtain a comprehensive derivation of (11), it is necessary to determine $\psi_j(x, y)$. Indeed, in regions 1, 3 and 5 there is only pristine graphene, then the corresponding eigenspinors can be written as [27, 29, 43]

$$\Psi_1(x, y, t) = \sum_{l,m=-\infty}^{+\infty} \left[\begin{pmatrix} 1 \\ \gamma_l \end{pmatrix} \delta_{m,0} e^{ik_x^0 x} + r_l \begin{pmatrix} 1 \\ -\gamma_l^* \end{pmatrix} e^{-ik_x^l x} \right] e^{ik_y y} \delta_{m,l} e^{-iv_F(\varepsilon + m\varpi)t} \quad (12)$$

$$\Psi_3(x, y, t) = \sum_{l,m=-\infty}^{+\infty} \left[c_{1l} \begin{pmatrix} 1 \\ \gamma_l \end{pmatrix} e^{ik_x^l x} + c_{2l} \begin{pmatrix} 1 \\ -\gamma_l^* \end{pmatrix} e^{-ik_x^l x} \right] e^{ik_y y} \delta_{m,l} e^{-iv_F(\varepsilon + m\varpi)t} \quad (13)$$

$$\Psi_5(x, y, t) = \sum_{l,m=-\infty}^{+\infty} \left[t_l \begin{pmatrix} 1 \\ \gamma_l \end{pmatrix} e^{ik_x^l x} + 0_l \begin{pmatrix} 1 \\ -\gamma_l^* \end{pmatrix} e^{-ik_x^l x} \right] e^{ik_y y} \delta_{m,l} e^{-iv_F(\varepsilon + m\varpi)t} \quad (14)$$

and the associated energy is

$$\varepsilon + l\varpi = s_l \sqrt{(k_x^l)^2 + k_y^2} \quad (15)$$

where $\varpi = \frac{\omega}{v_F}$, $\gamma_l = s_l \frac{k_x^l + ik_y}{\sqrt{(k_x^l)^2 + k_y^2}} = s_l e^{i\theta_l}$, $\theta_l = \arctan \frac{k_y}{k_x^l}$, $\delta_{m,l} = J_{m-l}(0)$, $s_l = \text{sgn}(\varepsilon + l\varpi)$, 0_l is the null vector, and c_{il} ($i = 1, 2$) are two constants. The coefficients r_l and t_l represent the reflection and transmission amplitudes, and their derivation will be provided in Appendix A.

In both regions 2 and 4, where laser fields are applied, the eigenvalue equation yields

$$(-i\partial_x - i(k_y - m\varpi)) \varphi_{2j}(x, y) = (\varepsilon + m\varpi) \varphi_{1j}(x, y) \quad (16)$$

$$(-i\partial_x + i(k_y - m\varpi)) \varphi_{1j}(x, y) = (\varepsilon + m\varpi) \varphi_{2j}(x, y) \quad (17)$$

which can be further analyzed to arrive at the solutions

$$\Psi_2(x, y, t) = \sum_{l,m=-\infty}^{+\infty} \left[a_{1l} \begin{pmatrix} 1 \\ \Gamma_l \end{pmatrix} e^{iq_x^l x} + a_{2l} \begin{pmatrix} 1 \\ -\Gamma_l^* \end{pmatrix} e^{-iq_x^l x} \right] e^{ik_y y} J_{m-l}(\alpha_2) e^{-iv_F(\varepsilon + m\varpi)t} \quad (18)$$

$$\Psi_4(x, y, t) = \sum_{l,m=-\infty}^{+\infty} \left[b_{1l} \begin{pmatrix} 1 \\ \Gamma_l \end{pmatrix} e^{iq_x^l x} + b_{2l} \begin{pmatrix} 1 \\ -\Gamma_l^* \end{pmatrix} e^{-iq_x^l x} \right] e^{ik_y y} J_{m-l}(\alpha_4) e^{-iv_F(\varepsilon + m\varpi)t} e^{-i(m-l)\beta} \quad (19)$$

and the corresponding energy is

$$\varepsilon + l\varpi = s_l \sqrt{(q_x^l)^2 + (k_y - l\varpi)^2} \quad (20)$$

where we have defined $\Gamma_l = s_l \frac{q_x^l + i(k_y - l\varpi)}{\sqrt{(q_x^l)^2 + (k_y - l\varpi)^2}} = s_l e^{i\theta_l}$. The coefficients a_{il} and b_{il} ($i = 1, 2$) are four constants. It is noteworthy that the x -component q_x^l of the wave vector undergoes modification due to the laser field, in contrast to the scenario observed in the case of an oscillating barrier [28, 29, 45].

III. TRANSMISSION MODES

In Appendix A, we have determined all transmission modes and the associated total transmission. Then, according to (A30) and (A31), we have

$$T_m = \frac{\cos \theta_m}{\cos \theta_0} |t_m|^2 \quad (21)$$

$$T = \sum_{m=-N}^N T_m \quad (22)$$

where $\cos \theta_m = \frac{k_x^m}{\sqrt{(k_x^m)^2 + k_y^2}}$ and $k_x^m = \sqrt{(\varepsilon + m\varpi)^2 - k_y^2}$. To gain a comprehensive understanding of how two time-oscillating laser barriers influence Dirac fermions in graphene, we numerically simulate our results. The oscillation of the barriers generates multiple energy bands, indicating infinite transmission modes. This includes zero-photon transmission corresponding to the central energy band ε , as well as photon-assisted transmission aligned with sidebands at $\varepsilon + l\varpi$. For simplifying the graphical representation, we focus on the first three bands: the central band and the first two sidebands. Numerical simulation allows probing transmission dynamics across these bands to elucidate the impact of tunneling and photon exchange processes on Dirac fermion transport induced by the double laser barrier structure.

Fig. 2 depicts the transmissions as a function of the energy ε for various values of d_1 and d_2 , where d_1 is the distance between the two barriers of width $d_2 - d_1$. We take into account the condition $\varepsilon > k_y + 2\varpi$ in order to have transmission, and we mention that the quantity $k_y + 2\varpi$ serves as an effective mass [46]. We observe that the transmissions vary in an oscillatory way, and the total transmission oscillates in the vicinity of unity. Fig. 2a plotted for $d_1 = 3$ and $d_2 = 5$, we see that the transmission with photon emission T_1 (red line) decreases exponentially, the transmission with absorption T_{-1} (green line) increases along the ε -axis, and the transmission T_0 with zero photon exchange (blue line) decreases rapidly towards zero. When d_2 is increased, T_{-1} becomes null from $\varepsilon = 7$ but T_1 increases, and T_0 shows different behaviors varying between decreasing then increasing along the ε -axis as depicted in Fig. 2b. For the values $d_1 = 1$ and $d_2 = 5$, T_1 is almost zero for all energies, T_{-1} increases then decreases exponentially, and T_0 shows the opposite behavior (decreases then increases exponentially). From the value $\varepsilon = 10$, we see that the transmission is carried out only with zero photon exchange (T_0) and then all fermions cross the barrier, showing perfect transmission. For $d_2 = 10$ in Fig. 2d, we observe that T_0 is dominant between $\varepsilon = 6$ and $\varepsilon = 9$, and after that, T_1 becomes more dominant but T_{-1} is almost null. In conclusion, the modulation of the two distances d_1 and d_2 serves as a means to control transmission modes, consistent with observations for time-oscillating barriers [27]. Notably, adjusting one of the two distances can influence transmission properties. However, it is important to highlight that complete suppression of Klein tunneling is not achievable in graphene. Overall, the separation between laser-induced barriers emerges as a design parameter offering tunable transmission through the graphene sheet, with Klein tunneling persisting as an underlying effect shaped by the massless nature of Dirac fermions.

In Fig. 3, we plot the transmission T_0 of the central band ($l = 0$) as a function of the energy ε for different values of d_1 and d_2 . Fig. 3a illustrates the behavior of T_0 for three values $d_1 = 1, 5, 9$. It is evident that as d_1 increases, the number of oscillations also increases, and T_0 becomes more dominant in the contribution to the total transmission because the two barriers resemble two peaks of width $d = d_2 - d_1$. In this scenario, a majority of incident fermions traverse the barrier with zero photon exchange, as evident in the green curve corresponding to $d_1 = 9$. Now for $d_2 = 2, 6, 9$, we present T_0 in Fig. 3b. We observe that for $d_2 = 4$ (red line), T_0 is very weak and decreases in an oscillatory way. For $d_2 = 6$ (green line), T_0 increases for low energies, then decreases exponentially towards zero in the vicinity of $\varepsilon = 11$. For $d_2 = 9$ (blue line), T_0 becomes more important than the other transmission process because the sum of the three transmission modes is close to unity. We can conclude that increasing the width of barriers d suppresses the transmission of the side bands and increases the transmission with zero photon exchange.

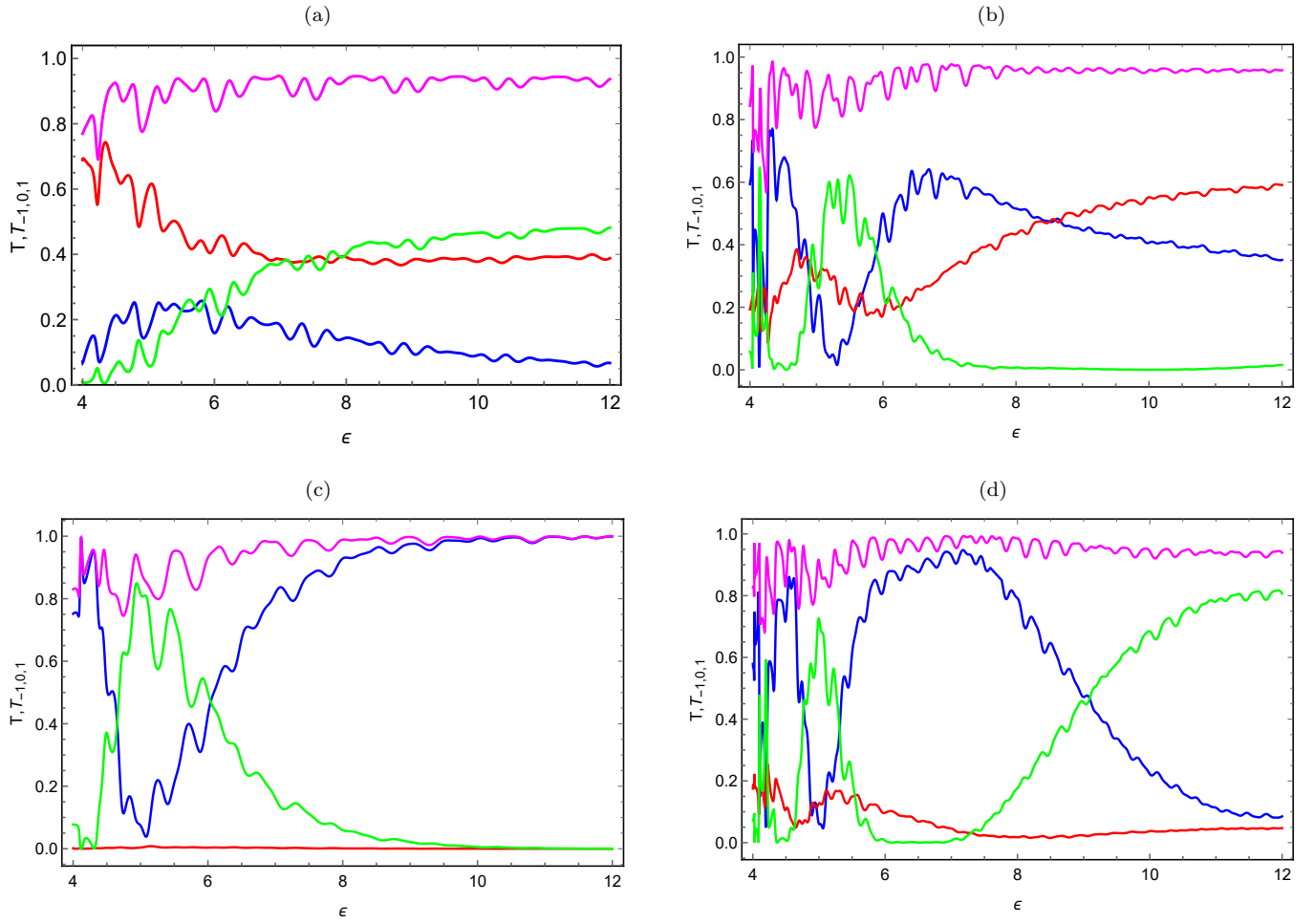


FIG. 2. (Color online) Transmissions as a function of the energy ϵ for $\omega = 1.5$, $k_y = 1$, $\beta = \frac{\pi}{8}$, $F_2 = F_4 = 1.5$, and different distances (d_1, d_2) with (a): $d_1 = 3$, $d_2 = 5$, (b): $d_1 = 3$, $d_2 = 10$, (c): $d_1 = 1$, $d_2 = 5$, (d): $d_1 = 1$, $d_2 = 10$. T_1 (red line), T_{-1} (green line), T_0 (blue line), and T (magenta line).

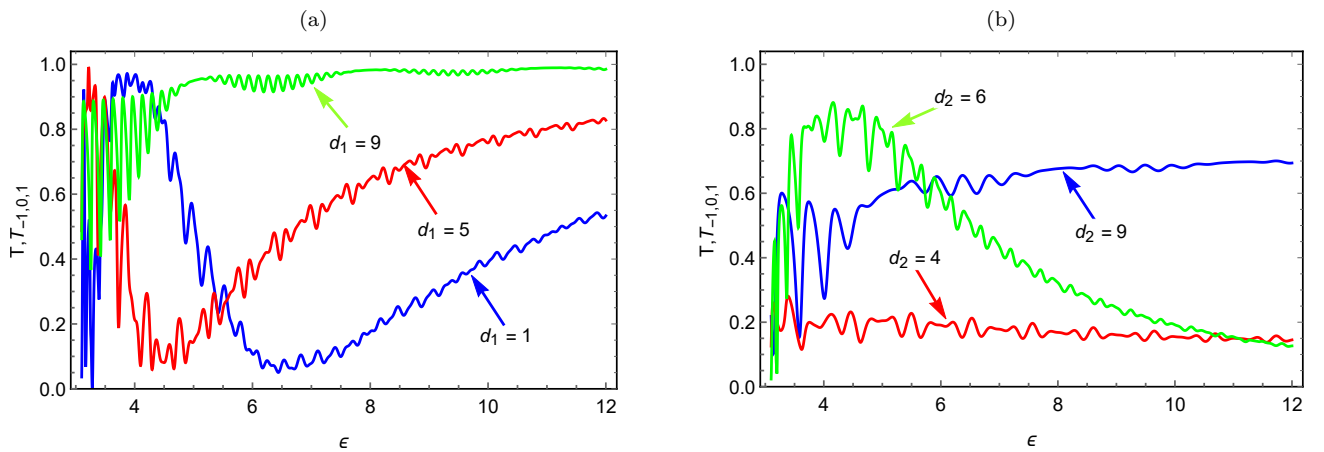


FIG. 3. (Color online) Transmission T_0 with zero photon exchange as a function of the energy ϵ for $\beta = 0$, $k_y = 0.1$, $\varpi = 1.5$, $F_2 = F_4 = 1.5$, and different distances (d_1, d_2) with (a): $d_2 = 10$, $d_1 = 1$ (blue line), $d_1 = 5$ (red line), $d_1 = 9$ (green line), and (b): $d_1 = 3$, $d_2 = 4$ (blue line), $d_2 = 6$ (red line), $d_2 = 9$ (green line).

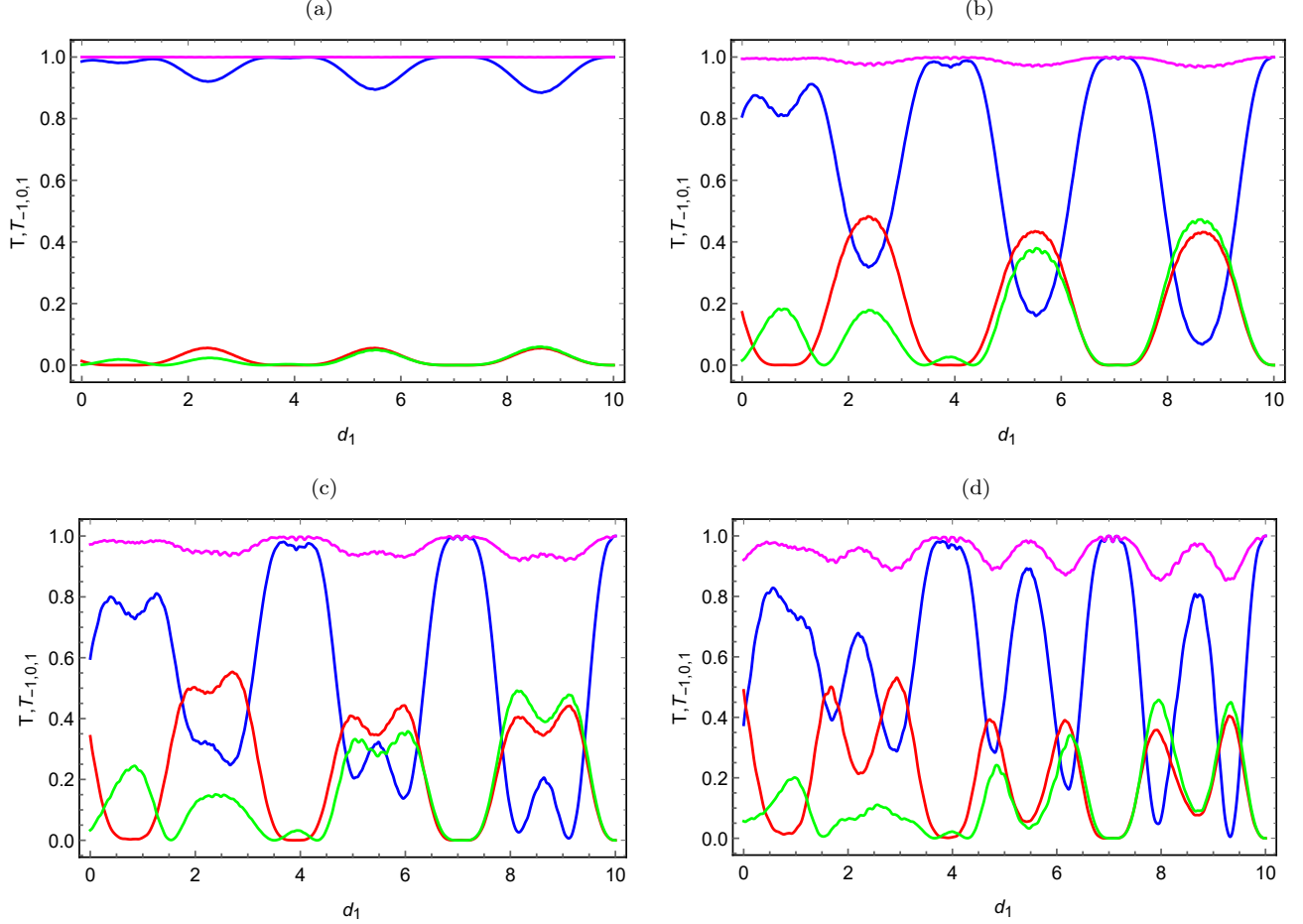


FIG. 4. (Color online) Transmissions as a function of the distance d_1 , separating two barriers, for $d_2 = 10$, $k_y = 1$, $\varpi = 2$, $\varepsilon = 20$, $\beta = 0$, and different amplitudes F ($F_1 = F_4 = F$) with (a): $F = 0.5$, (b): $F = 1.9$, (c): $F = 2.9$, (d): $F = 3.9$. With T (magenta line), T_0 (blue line), T_1 (red line), T_{-1} (green line).

In Fig. 4, we present the transmissions as a function of the distance d_1 between the two barriers for different values of the amplitude F of the laser field. For $F = 0.5$ in Fig. 4a, we observe that the total transmission T (magenta line) almost equals unit whatever the distance d_1 because the laser fields are very weak and they have almost a negligible effect. The transmission T_0 with zero photon exchange oscillates in the vicinity of the unit, and the transmissions (T_1 , T_{-1}) with photon exchange oscillate in the vicinity of zero. The laser fields are very weak but allow for quantifying the energy, even though the majority of the fermions cross the barrier with zero photon exchange. For $F = 1.9$ in Fig. 4b, we see that the laser effect is very clear because T_0 varies periodically, T_1 (red line) decreases, and T_{-1} increases along the d_1 -axis. However, T_0 varies in phase opposition with the two other transmission modes, with an increase in the amplitude of the oscillations along the d_1 -axis. The total transmission remains consistently close to unity, demonstrating the transparency of two barriers. indicating barrier transparency. For $F = 2.9$ in Figure 4c, T_0 exhibits oscillations with an amplification in amplitude, and it diminishes for specific values. For $F = 3.9$ in Fig. 4d, a reduction in the interval where T_1 and T_{-1} are canceled is observed, accompanied by an increase in the number of peaks. It is noticeable that T_1 oscillates with a decrease in amplitude while T_{-1} increases. Consequently, increasing the amplitude F of the laser fields seems to reduce the interval of transmission cancellation, but it also leads to an increase in the number of oscillations.

Fig. 5 presents transmissions as a function of the distance d_2 for a fixed d_1 , where $d_2 - d_1$ is the width of two barriers. for the same configuration of parameters taken in Fig. 4. For $F = 0.5$ in Fig. 5a, we observe a generation of transmission modes, but the effect of the laser fields is very weak. The transmissions T_1 and T_{-1} oscillate around zero, which can be neglected compared to the contribution of T_0 , implying perfect transmission. For $F = 1.9$ in Fig. 5b, we notice that T_1 and T_{-1} vary periodically with an increase in amplitude, but T_0 varies in an oscillatory way with a decrease in the amplitude. For $F = 2.9$, Fig. 5c shows that T_0 varies regularly with an appearance of peaks in

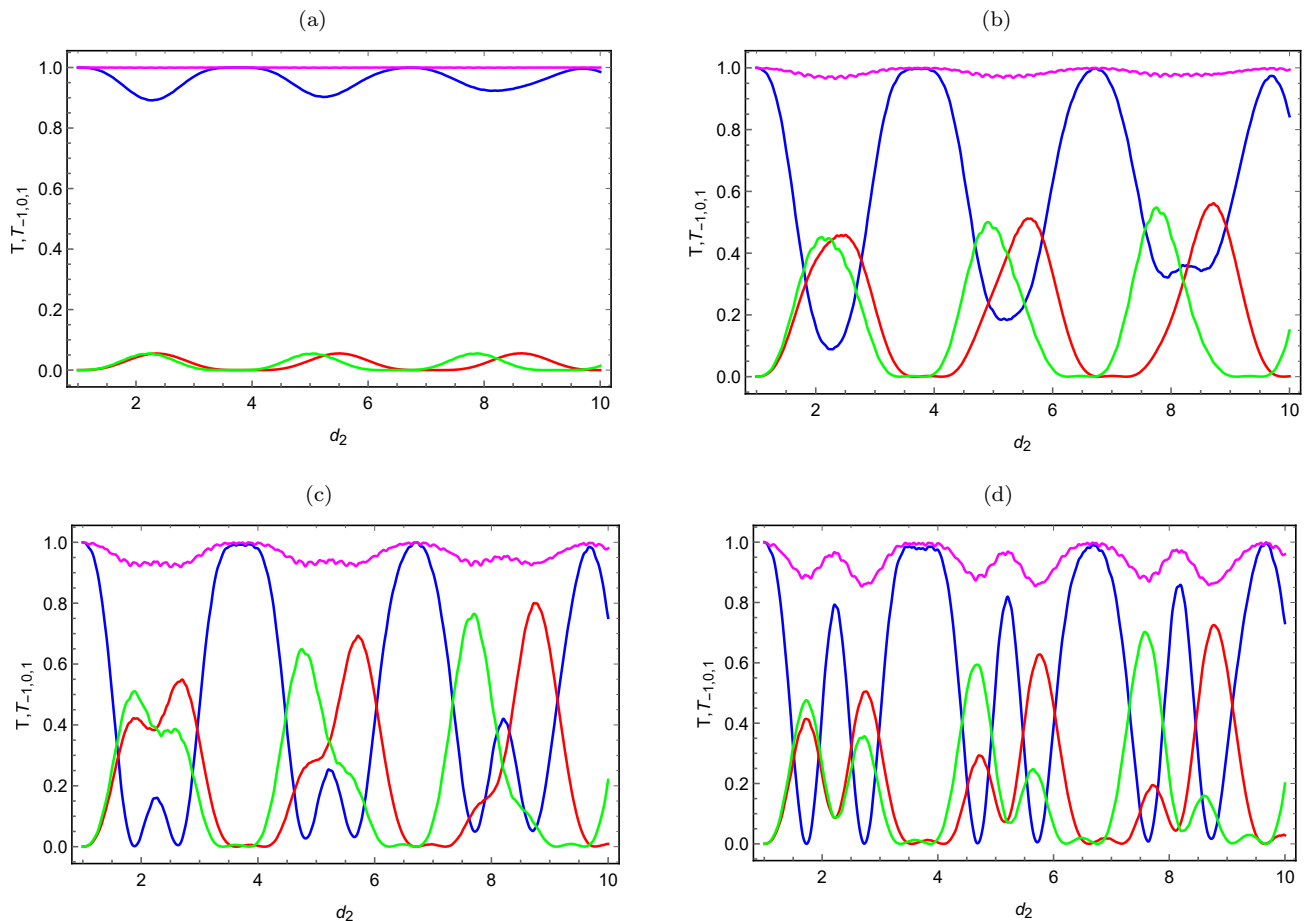


FIG. 5. (Color online) Transmissions as a function of the distance d_2 , for $d_1 = 1$, $k_y = 1$, $\varpi = 2$, $\varepsilon = 20$, $\beta = 0$, and different amplitudes F ($F_2 = F_4 = F$) with (a): $F = 0.5$, (b): $F = 1.9$, (c): $F = 2.9$, (d): $F = 3.9$. With T (magenta line), T_0 (blue line), T_1 (red line), T_{-1} (green line).

the minimum part. For $F = 3.9$ in Fig. 5d, we observe that the total transmission T oscillates around the unit, while T_0 is more dominant, oscillating between zero and one, canceling out at several points. T_1 and T_{-1} also oscillate with an increase in amplitude. For example, in the vicinity of the value $d_2 = 4$, T_1 and T_{-1} are almost null, but T_0 is equal to the unit, which implies that all the fermions cross the barrier without exchanging photons.

In Fig. 6, we show transmissions as a function of the phase shift β for $k_y = 1$, $\varpi = 2$, $\varepsilon = 12$, $F_2 = 2$, $d_1 = 1.3$, $d_2 = 3$, and various amplitudes F_4 of the second laser barrier. In Fig. 6a with $F_4 = 0.9$, we notice that the three transmission modes (T_0, T_1, T_{-1}) exhibit consistent oscillations with the same frequency across different amplitudes. Notably, T_0 (zero photon) appears more predominant, while T_1 (photon emission) and T_{-1} (photon absorption) exhibit similar variations. These two transmissions periodically nullify for specific values of β , resembling observations in the case of time-oscillating barriers [27]. The total transmission T oscillates around unity, and then two barriers are transparent. In Fig. 6b with $F_4 = 2$, we observe that the amplitude of oscillations gets intensified, while T exhibits fluctuations around unity with a dominance of T_0 . In Fig. 6c with $F_4 = 2.9$, transmissions vary periodically by losing the sinusoidal behavior, and even the periodicity gets lost for some particular values of β . In this setup, T_0 maintains a dominant presence, exhibiting an amplitude close to 0.9, while T_1 and T_{-1} undergo symmetrical variations. For $F_4 = 3.9$, Fig. 6d illustrates a decrease in the amplitude of T_0 with a simultaneous increase in the number of oscillations, leading to periodic cancellations. The three transmissions become nearly equiprobable, and the periodic observation of perfect transmission occurs.

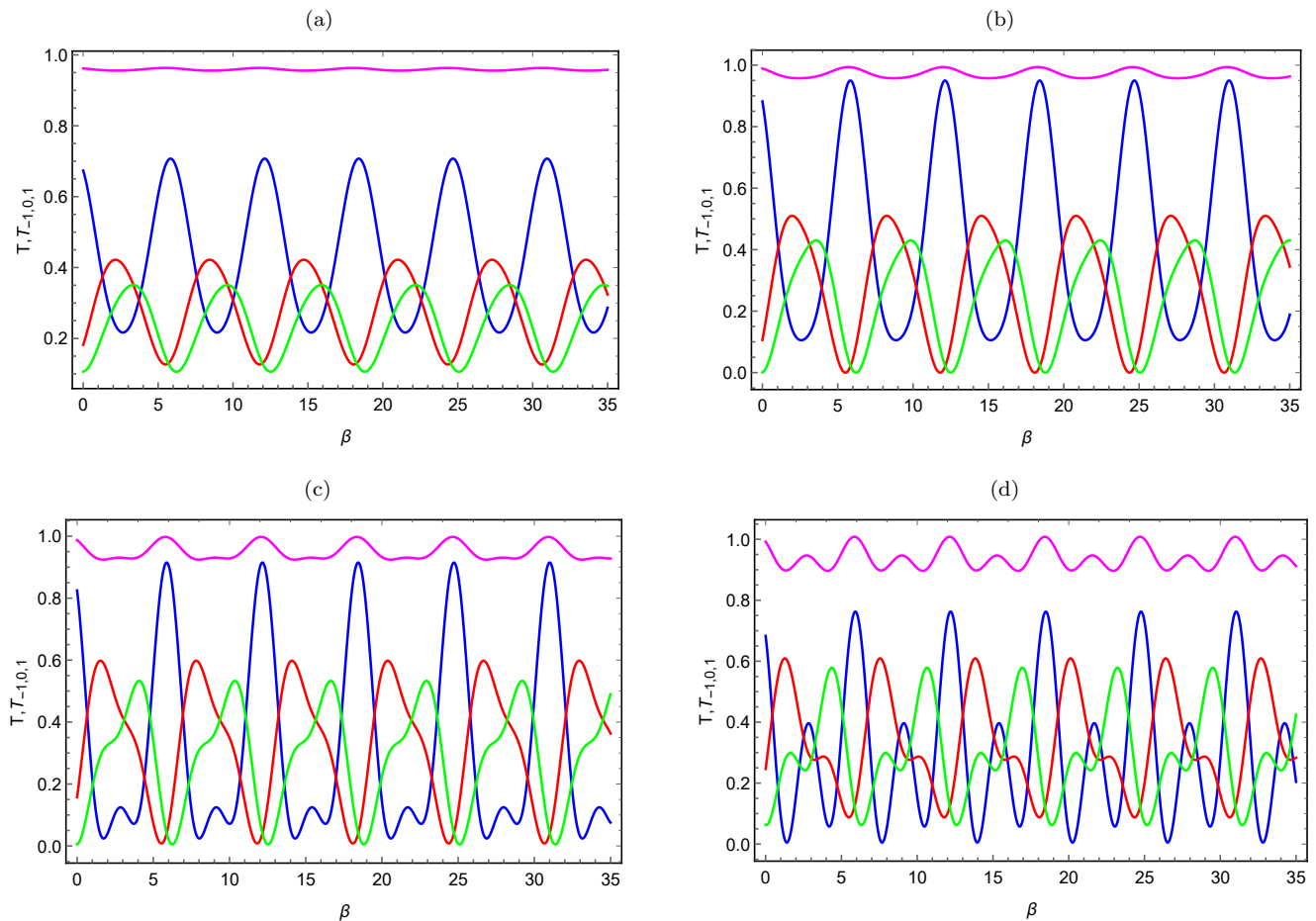


FIG. 6. (Color online) Transmissions as a function of the phase shift β for $k_y = 1$, $\varpi = 2$, $\varepsilon = 12$, $F_2 = 2$, $d_1 = 1.3$, $d_2 = 3$, and different value of amplitude F_4 such that (a): $F_4 = 0.9$, (b): $F_4 = 2$, (c): $F_4 = 2.9$, (d): $F_4 = 3.9$. With T (magenta line), T_0 (blue line), T_1 (red line), T_{-1} (green line).

IV. CONCLUSION

We have studied the transmission of Dirac fermions through double laser barriers generated by two electric fields of amplitude (F_2, F_4) and frequency ω shifted by a phase shift β . The two barriers divide the graphene sheet into five regions, such that in regions 1, 3, and 5, there is only pristine graphene, and the other two regions are irradiated by laser fields. By using the Floquet approximation, we analytically determined the eigenspinors associated with each region. Additionally, we showed that the oscillation of the barriers over time generates several energy bands denoted by $\varepsilon + l\varpi$ with $l = 0, \pm 1, \dots$. Subsequently, we have determined the transmission modes by applying the boundary conditions at the interfaces of the two barriers and using the transfer matrix method together with current density.

For numerical illustrations, we restricted ourselves to the three first modes corresponding to the central band ε and the first two side bands correspond to the $\varepsilon \pm \varpi$. We showed that the transmission exists if the incident energy of the Dirac fermions satisfies the condition $\varepsilon > k_y + 2\varpi$. It was observed that the time-varying barrier induces two transmission processes: one without and one with photon exchanges. It was demonstrated that varying the distance d_1 , which separates the two barriers, offers a means to cancel one of the two transmission processes, modify the number of oscillations, and adjust the transmission processes. It was observed that an increase in d_1 results in a higher number of oscillations. This is attributed to additional resonance between the barriers and the quasi-confined states, activating the transmission process with zero photon exchange while suppressing the transmission processes involving photon exchange. Reducing the distance d_2 leads to a decrease in the transmission T_0 with zero photon exchange, even as the incident energy ε increases. An increase in the laser field amplitude raises both the number of oscillations and their associated amplitude. Periodic observation of perfect transmission is noted, occurring for very precise values of the phase shift β .

This study serves as a crucial step in laying the groundwork for the development of optoelectronic technologies utilizing photon-assisted tunneling in graphene. By advancing our understanding of light-matter interactions at the nanoscale, the current research establishes a foundation for the future application of graphene in devices driven by transient optical fields. The insights gained from this study are poised to inspire further research aimed at harnessing photon-induced tunneling effects for diverse applications, including ultrafast optoelectronics, renewable energy generation, and quantum information systems that leverage the distinctive characteristics of Dirac fermions. In essence, this investigation contributes to enabling the translation of emerging nanophotonics concepts into new generations of innovative optoelectronic architectures, taking advantage of graphene's unique light-sensitive properties.

In the following, we discuss how to design a realistic experiment for the interaction of graphene electrons with a double barrier of laser beams. In real experimental scenarios, the generation of time-oscillating barriers requires the manipulation of external fields or potentials to alter the potential landscape experienced by particles or waves. Researchers typically use two methods for this purpose. The first method involves the use of an optical grating created by the interference of laser beams, resulting in the formation of a periodic potential [47, 48]. By carefully controlling the laser parameters, such as intensity and phase, the optical lattice can be tailored to create the desired time-varying barriers. The second method involves the application of time-dependent electric fields. By subjecting a device, such as a semiconductor heterostructure or microfabricated device, to a varying voltage, an electric field is induced. This time-dependent electric field can be modulated in a sinusoidal manner or shaped with other time-dependent waveforms [49, 50]. These variations in the electric field result in the formation of time-varying barriers, allowing researchers to study the interactions of particles or waves with this dynamic potential landscape.

ACKNOWLEDGMENT

We thank Prof. A. H. Alhaidari for valuable discussions.

CONFLICT OF INTEREST STATEMENT

The authors declare that they have no known competing financial interests or personal relationships that could have appeared to influence the work reported in this paper.

AUTHORS CONTRIBUTION STATEMENT

All authors have contributed equally to the paper.

DATA AVAILABILITY STATEMENT

The data that support the findings of this study are available on request from the corresponding author.

-
- [1] A. K. Geim and K. S. Novoselov, *Nat. Mater.* 6, 183 (2007).
 - [2] K. S. Novoselov, A. K. Geim, S. V. Morozov, D. Jiang, M. I. Katsnelson, I. V. Grigorieva, S. V. Dubonos, and A. A. Firsov, *Nature* 438, 197 (2005).
 - [3] K. S. Novoselov, A. K. Geim, S. V. Morozov, D. Jiang, Y. Zhang, S. V. Dubonos, I. V. Grigorieva, and A. A. Firsov, *Science* 306, 666 (2004).
 - [4] A. H. Castro Neto, F. Guinea, N. M. R. Peres, K. S. Novoselov, and A. K. Geim, *Rev. Mod. Phys.* 81, 109 (2009).
 - [5] A. K. Geim, *Science* 324, 1530 (2009).
 - [6] Y. Zhang, Y. W. Tan, H. L. Stormer, and P. Kim, *Nature* 438, 201 (2005).
 - [7] C. L. Kane and E. J. Mele, *Phys. Rev. Lett.* 95, 226801 (2005).
 - [8] S. Morozov, K. Novoselov, M. Katsnelson, F. Schedin, D. Elias, J. Jaszczak, and A. Geim, *Phys. Rev. Lett.* 100, 016602 (2008).
 - [9] K. I. Bolotin, K. J. Sikes, Z. Jiang, M. Klima, G. Fudenberg, J. Hone, P. Kim, and H. L. Stormer, *Solid State Commun.* 351, 146 (2008).
 - [10] Qiaoliang Bao, Han Zhang, Bing Wang, Zhenhua Ni, Candy Haley Yi Xuan Lim, Yu Wang, Ding Yuan Tang, and Kian Ping Loh, *Nat. Photonics* 5, 411 (2011).

- [11] S. Reich, J. Maultzsch, C. Thomsen, and P. Ordejon, *Phys. Rev. B* 66, 035412 (2002).
- [12] N. M. R. Peres, *J. Phys. Condens. Matter* 21, 323201 (2009).
- [13] M. I. Katsnelson, K. S. Novoselov, and A. K. Geim, *Nat. Phys.* 2, 620 (2006).
- [14] C. W. J. Beenakker, *Rev. Mod. Phys.* 80, 1337 (2008).
- [15] N. Stander, B. Huard, and D. Goldhaber-Gordon, *Phys. Rev. Lett.* 102, 026807 (2009).
- [16] A. N. Sidorov, M. M. Yazdanpanah, R. Jalilian, P. J. Ouseph, R. W. Cohn, and G. U. Sumanasekera, *Nanotechnol.* 18, 135301 (2007).
- [17] G. A. K. P. A. Giovannetti, P. A. Khomyakov, G. Brocks, V. V. Karpan, J. van den Brink, and P. J. Kelly, *Phys. Rev. Lett.* 101, 026803 (2008).
- [18] F. Guinea, M. I. Katsnelson, and A. K. Geim, *Nat. Phys.* 6, 30 (2010).
- [19] G.-X. Ni, Y. Zheng, S. Bae, H. R. Kim, A. Pachoud, Y. S. Kim, C.-L. Tan, D. Im, J.-H. Ahn, B. H. Hong, and B. Ozyilmaz, *ACS Nano* 6, 1158 (2012).
- [20] J. M. Pereira, F. M. Peeters, A. Chaves, and G. A. Farias, *Semicond. Sci. Technol.* 25 033002 (2010).
- [21] C. Bai and X. Zhang, *Phys. Rev. B* 76, 075430 (2007).
- [22] L. Sun and Y. Guo, *J. Appl. Phys.* 109, 12 (2011).
- [23] A. De Martino, L. Dell'Anna, and R. Egger, *Solid State Communi.* 144, 547 (2007).
- [24] L. Dell'Anna and A. De Martino, *Phys. Rev. B* 79, 045420 (2009).
- [25] M. R. Masir, P. Vasilopoulos, and F. M. Peeters, *New J. Phys.* 11, 095009 (2009).
- [26] Wenjun Li and L. E. Reichl, *Phys. Rev. B* 60, 15732 (1999).
- [27] H. P. Ojeda-Collado and C. Rodríguez-Castellanos, *Appl. Phys. Lett.* 103, 033110 (2013).
- [28] M. Ahsan Zeb, K. Sabeeh, and M. Tahir, *Phys. Rev. B* 78, 165420 (2008).
- [29] C. Zhang and N. Tzoar, *Appl. Phys. Lett.* 53, 1982 (1988).
- [30] M. Moskalets and M. Büttiker, *Phys. Rev. B* 68, 075303 (2003).
- [31] R. Biswas, S. Maitty, and C. Sinha, *Physica E* 84, 235 (2016).
- [32] R. Biswas and C. Sinha, *Appl. Phys.* 114, 183706 (2013).
- [33] R. El Aitouni, M. Mekkaoui, and A. Jellal, *Ann. Phys. (Berlin)* 535, 2200630 (2023).
- [34] R. El Aitouni and A. Jellal, *Phys. Lett. A.* 447, 128288 (2022).
- [35] S. E. Savel'ev and A. S. Alexandrov, *Phys. Rev. B* 84, 035428 (2011).
- [36] I. Gierz, E. Hendry, and M. Orlita, *Nat. Mat.* 12, 1119 (2013).
- [37] P. Ruffieux, S. Wang, B. Yang, C. Sánchez-Sánchez, J. Liu, T. Dienel, et al., *Nature* 531(7595), 489 (2016).
- [38] Z. Fang, S. Thongrattanasiri, A. Schlather, Z. Liu, L. Ma, Y. Wang, et al., *ACS Nano* 7(3), 2388 (2013).
- [39] K. F. Mak, C. Lee, J. Hone, J. Shan, and T. F. Heinz, *Phys. Rev. Lett.* 105, 136805 (2010).
- [40] Q. H. Wang, K. Kalantar-Zadeh, and A. Kis, *Rev. Mod. Phys.* 84, 1317 (2012).
- [41] S. Iijima, *Nature* 354, 56 (1991).
- [42] R. Loudon, *The Quantum Theory of Light*, 3rd ed. (Oxford University Press Inc., New York, 2000).
- [43] Z. Li, J. Wu and K. S. Chan, *Phys. Lett. A*, 376, 1159 (2012).
- [44] J. H. Shirley, *Phys. Rev.* 138, B979 (1965).
- [45] B. Trauzettel, Y. M. Blanter, and A. F. Morpurgo, *Phys. Rev. B* 75, 035305 (2007).
- [46] A. D. Alhaidari, A. Jellal, E. B. Choubabi, and H. Bahlouli, *Quantum Matter* 2, 140 (2013).
- [47] I. Bloch, *Nat. Phys.* 1, 23 (2005).
- [48] M. Lewenstein, A. Sanpera, V. Ahufinger, B. Damski, A. Sen(De), and U. Sen, *Adv. Phys.* 56, 243 (2007).
- [49] R. C. Ashoori, *Nature* 379, 413 (1996).
- [50] S. M. Reimann and M. Manninen, *Rev. Mod. Phys.* 74, 1283 (2002).

Appendix A: Transmission modes

To derive the transmission modes, we use the continuity of the eigenspinors at the barrier interfaces. Indeed, for the first barrier, we write $\Psi_1(-d_2, y, t) = \Psi_2(-d_2, y, t)$ and $\Psi_2(-d_1, y, t) = \Psi_3(-d_1, y, t)$, which allow us to get the

set of equations

$$\delta_{m,0}e^{-ik_x^0 d_2} + r_m e^{+ik_x^m d_2} = \sum_{l=-\infty}^{+\infty} \left(a_{1l} e^{-iq_x^l d_2} + a_{2l} e^{+iq_x^l d_2} \right) J_{m-l}(\alpha_2) \quad (\text{A1})$$

$$\delta_{m,0}\gamma_m e^{-ik_x^0 d_2} - r_m \gamma_m^* e^{+ik_x^m d_2} = \sum_{l=-\infty}^{+\infty} \left(a_{1l} \Gamma_l e^{-iq_x^l d_2} - a_{2l} \Gamma_l^* e^{+iq_x^l d_2} \right) J_{m-l}(\alpha_2) \quad (\text{A2})$$

$$c_{1m} e^{-ik_x^m d_1} + c_{2m} e^{+ik_x^m d_1} = \sum_{l=-\infty}^{+\infty} \left(a_{1l} e^{-iq_x^l d_1} + a_{2l} e^{+iq_x^l d_1} \right) J_{m-l}(\alpha_2) \quad (\text{A3})$$

$$c_{1m} \gamma_m e^{-ik_x^m d_1} - c_{2m} \gamma_m^* e^{+ik_x^m d_1} = \sum_{l=-\infty}^{+\infty} \left(a_{1l} \Gamma_l e^{-iq_x^l d_1} - a_{2l} \Gamma_l^* e^{+iq_x^l d_1} \right) J_{m-l}(\alpha_2). \quad (\text{A4})$$

As for the second barrier, we have $\Psi_3(d_1, y, t) = \Psi_4(d_1, y, t)$ and $\Psi_4(d_2, y, t) = \Psi_5(d_2, y, t)$, then we end up with the following set

$$c_{1m} e^{ik_x^m d_1} + c_{2m} e^{-ik_x^m d_1} = \sum_{l=-\infty}^{+\infty} \left(b_{1l} e^{iq_x^l d_1} + b_{2l} e^{-iq_x^l d_1} \right) e^{-i(m-l)\beta} J_{m-l}(\alpha_4) \quad (\text{A5})$$

$$c_{1m} \gamma_m e^{ik_x^m d_1} - c_{2m} \gamma_m^* e^{-ik_x^m d_1} = \sum_{l=-\infty}^{+\infty} \left(b_{1l} \Gamma_l e^{iq_x^l d_1} - b_{2l} \Gamma_l^* e^{-iq_x^l d_1} \right) e^{-i(m-l)\beta} J_{m-l}(\alpha_4) \quad (\text{A6})$$

$$t_m e^{ik_x^m d_2} + 0_m e^{-ik_x^m d_2} = \sum_{l=-\infty}^{+\infty} \left(b_{1l} e^{iq_x^l d_2} + b_{2l} e^{-iq_x^l d_2} \right) e^{-i(m-l)\beta} J_{m-l}(\alpha_4) \quad (\text{A7})$$

$$t_m \gamma_m e^{ik_x^m d_2} - 0_m \gamma_m^* e^{-ik_x^m d_2} = \sum_{l=-\infty}^{+\infty} \left(b_{1l} \Gamma_l e^{iq_x^l d_2} - b_{2l} \Gamma_l^* e^{-iq_x^l d_2} \right) e^{-i(m-l)\beta} J_{m-l}(\alpha_4). \quad (\text{A8})$$

The above sets can be mapped in the matrix form

$$\begin{pmatrix} \delta_{m,0} \\ r_m \end{pmatrix} = \begin{pmatrix} \mathbb{S}_{1,1} & \mathbb{S}_{1,2} \\ \mathbb{S}_{2,1} & \mathbb{S}_{2,2} \end{pmatrix} \begin{pmatrix} t_m \\ 0_m \end{pmatrix} = \mathbb{S} \begin{pmatrix} t_m \\ 0_m \end{pmatrix} \quad (\text{A9})$$

where \mathbb{S} is the transfer matrix. It is essential to note that \mathbb{S} has infinite order, and for simplification, we truncate it to finite order by considering m between $-N$ and N , where $N > \alpha_j$ [26, 28]. \mathbb{S} is expressed as a product of the transfer matrix $\mathbb{S}(j, j+1)$ from region j to region $j+1$

$$\mathbb{S} = \mathbb{S}(1, 2) \cdot \mathbb{S}(2, 3) \cdot \mathbb{S}(3, 4) \cdot \mathbb{S}(4, 5) \quad (\text{A10})$$

with different matrices

$$\mathbb{S}(1, 2) = \begin{pmatrix} \mathbb{G}_{-d_2}^0 & \mathbb{G}_{d_2} \\ \mathbb{R}_{+,-d_2}^{+1} & \mathbb{R}_{-,d_2}^{-1} \end{pmatrix}^{-1} \begin{pmatrix} \mathbb{H}_{+,d_2}^2 & \mathbb{H}_{+,-d_2}^2 \\ \mathbb{L}_{+,-d_2}^{2,+1} & \mathbb{L}_{-,d_2}^{2,-1} \end{pmatrix} \quad (\text{A11})$$

$$\mathbb{S}(2, 3) = \begin{pmatrix} \mathbb{H}_{+,-d_1}^2 & \mathbb{H}_{+,d_1}^2 \\ \mathbb{L}_{+,-d_1}^{2,+1} & \mathbb{L}_{-,d_1}^{2,-1} \end{pmatrix}^{-1} \begin{pmatrix} \mathbb{G}_{-d_1} & \mathbb{G}_{d_1} \\ \mathbb{R}_{+,-d_1}^{l,+1} & \mathbb{R}_{-,d_1}^{l,-1} \end{pmatrix} \quad (\text{A12})$$

$$\mathbb{S}(3, 4) = \begin{pmatrix} \mathbb{G}_{d_1} & \mathbb{G}_{-d_1} \\ \mathbb{R}_{+,d_1}^{+1} & \mathbb{R}_{-,-d_1}^{-1} \end{pmatrix}^{-1} \begin{pmatrix} \mathbb{K}_{+,-d_1}^4 & \mathbb{K}_{+,d_1}^4 \\ \mathbb{F}_{+,d_1}^{4,+} & \mathbb{F}_{-,-d_1}^{4,+} \end{pmatrix} \quad (\text{A13})$$

$$\mathbb{S}(4, 5) = \begin{pmatrix} \mathbb{K}_{+,-d_2}^4 & \mathbb{K}_{+,-d_2}^4 \\ \mathbb{F}_{+,d_2}^{4,+} & \mathbb{F}_{-,-d_2}^{4,+} \end{pmatrix}^{-1} \begin{pmatrix} \mathbb{G}_{d_2} & \mathbb{G}_{-d_2} \\ \mathbb{R}_{+,d_2}^{+1} & \mathbb{R}_{-,-d_2}^{-1} \end{pmatrix} \quad (\text{A14})$$

where $z = \pm d_{1,2}$ and we have set

$$(\mathbb{G}_z^0) = e^{ik_x^0 z} \quad (\text{A15})$$

$$(\mathbb{G}_z)_{m,l} = e^{ik_x^l z} \delta_{m,l} \quad (\text{A16})$$

$$(\mathbb{R}_{\pm,z}^{\pm 1})_{m,l} = \pm \gamma_l^{\pm 1} e^{ik_x^l z} \delta_{m,l} \quad (\text{A17})$$

$$(\mathbb{H}_{\pm,z}^j)_{m,l} = \pm e^{iq_x^l z} J_{m-l}(\alpha_j) \quad (\text{A18})$$

$$(\mathbb{L}_{\pm,z}^{j,\pm 1})_{m,l} = \pm \Gamma_l^{\pm 1} e^{iq_x^l z} J_{m-l}(\alpha_j) \quad (\text{A19})$$

$$(\mathbb{K}_{\pm,z}^j)_{m,l} = \pm e^{iq_x^l z} J_{m-l}(\alpha_j) e^{-i(m-l)\beta} \quad (\text{A20})$$

$$(\mathbb{F}_{\pm,z}^{j,\pm 1})_{m,l} = \pm \Gamma_l^{\pm 1} e^{iq_x^l z} J_{m-l}(\alpha_j) e^{-i(m-l)\beta}. \quad (\text{A21})$$

We assume the electron propagation direction is from left to right with energy ε along x -direction, therefore, the transmission coefficient of the m -th band is written as follows:

$$t_m = S' \delta_{m,0} \quad (\text{A22})$$

with $S' = S_{1,1}^{-1}$. Recall that m varies from $-N$ to N , that is to say

$$\begin{pmatrix} t_{-N} \\ \cdot \\ \cdot \\ t_{-1} \\ t_0 \\ t_1 \\ \cdot \\ \cdot \\ t_N \end{pmatrix} = S' \begin{pmatrix} 0 \\ \cdot \\ \cdot \\ 0 \\ 1 \\ 0 \\ \cdot \\ \cdot \\ 0 \end{pmatrix}. \quad (\text{A23})$$

To simplify, we limit our study to the three first bands: the central band ε and the two first side bands $\varepsilon \pm \varpi$. In this case, we obtain

$$t_{-1} = S'[1, 2] \quad (\text{A24})$$

$$t_0 = S'[2, 2] \quad (\text{A25})$$

$$t_1 = S'[3, 2]. \quad (\text{A26})$$

The transmission probability can be derived from the current density $J = \Psi^\dagger \sigma_x \Psi$, obtained from the continuity equation. As a result, the incident, reflected, and transmitted densities are given by

$$J_{\text{inc}}^0 = \gamma_0 + \gamma_0^* \quad (\text{A27})$$

$$J_{\text{ref}}^m = r_m r_m^* (\Gamma_m + \Gamma_m^*) \quad (\text{A28})$$

$$J_{\text{tra}}^m = t_m t_m^* (\gamma_m + \gamma_m^*) \quad (\text{A29})$$

where $\gamma_m = s_m \frac{k_x^m + i(k_y - m\omega)}{\sqrt{(k_x^m)^2 + (k_y - m\omega)^2}}$ and $\Gamma_m = s_m \frac{q_x^m + i(k_y - m\omega)}{\sqrt{(q_x^m)^2 + (k_y - m\omega)^2}}$. The transmission corresponding to the m -th side-band, is then write as

$$T_m = \frac{\cos \theta_m}{\cos \theta_0} |t_m|^2 \quad (\text{A30})$$

where $\cos \theta_m = \frac{k_x^m}{\sqrt{(k_x^m)^2 + k_y^2}}$ and $k_x^m = \sqrt{(\varepsilon + m\varpi)^2 - k_y^2}$. Finally, the total transmission is given by the sum over all modes

$$T = \sum_{m=-N}^N T_m. \quad (\text{A31})$$